Extracting Autofluorescence from Diffuse Optical Images

Frédéric Lesage
Coordinator, École Polytechnique de Montréal

Frédéric Leblond
Industrial representative, ART Inc.

Olesya Peshko
Report writer, McMaster University

Shidong Shan
Student, University of British Columbia

1. Introduction

The problem studied by the team was proposed by the company ART Advanced Research Technologies Inc., which "designs, develops, and markets optical imaging products for the medical and pharmaceutical industries" (see the web site `http://www.art.ca/en/art/profile.php`). Also, "ART has developed several products that relate to medical imaging, diagnostics, medical research and drug discovery". Among these products one finds Optix, "an *in vivo* optical molecular imaging device designed to monitor physiological changes in small animals during preclinical drug studies". Optix is used worldwide by industry and academic leaders. The students in the team, Olesya Peshko and Shidong Shan, were supposed to investigate the algorithms used in this product and their work led to the improvement of one aspect of the optical data processing carried out by Optix. In the rest of this section we discuss biomedical imaging in general. Section 2 describes the approaches investigated by the team and the results obtained.

The advent of new biomedical imaging techniques has brought significant progresses in how we image humans and animals. In particular, the emergence in the mainstream of new modalities, such as diffuse optical imaging (see [13], [8], [12], [4], [5]), has enabled researchers to image hemodynamics in vivo in a non-invasive fashion. The relatively low absorption and low scattering in the 600-1000 nm spectral range allow detection of photons travelling through several centimetres of biological tissue. Coupled with accurate models of light propagation, the NIR (Near Infra-Red) techniques enable imaging of deep tissue with boundary measurements using non-ionizing, low dose radiation. Applications of clinical significance have emerged for this modality; among those, breast cancer detection and neuronal activation measurement for cognitive studies are applications currently being actively pursued. In particular, optical imaging is currently arousing interest in the neurosciences. Absorption of near infra-red light by blood (oxy- and deoxy-haemoglobin), see [13], [8], and [12], can be used to measure functional information during brain activation. For example, using different wavelengths, it is possible to map changes in hemodynamics and oxygenation levels to changes in light intensity during some neuronal task (see [4] and [5]). The advantages of this modality are that one can distinguish between oxygenated and deoxygenated blood, and that NIR techniques are more convenient and lightweight. Its main weaknesses concern spatial resolution and quantification.

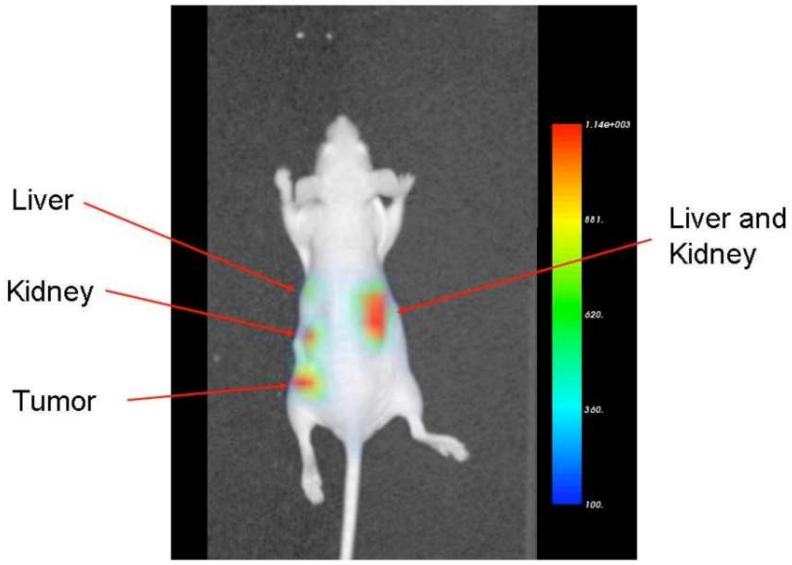

Figure 1. Small animal imaging with fluorescent probes targeting cancer

In parallel, associated with the emergence of endogenous diffuse optical imaging in humans, a new approach is emerging that enables to follow molecular products injected in animals, in vivo, through fluorescence. This new imaging technique (see [6], [9], [14], and [3]), referred to as molecular imaging, holds great promises: whereas one would detect diseases through anatomical changes and anomalies, we can now use new methods to provide a minimally invasive characterization and measurement of biological processes at the cellular and molecular levels of living organisms. Applications abound: early detection of diseases, real-time assessment of therapy effectiveness, and specific and selective delivery of drugs to targeted tissues. The recent emergence of genomic information clears the way for more individualized and specific drugs. Angiogenesis, hypoxia and pH, hyper-metabolism, micro-calcifications, and protein expression are all potential targets for these new techniques. Optical biomedical imaging has, over the last few years, enabled researchers to take significant steps towards this new paradigm. Fluorescent optical imaging, however, is subject to inherent difficulties. Tissues also generate fluorescence, and one needs to determine whether the measurements originate from the molecular compound that was injected or from autofluorescence.

Whether it is necessary to localize structures originating from targeted inclusions in the images or to filter out autofluorescence to improve image quality, the problem consists of segmenting out components of the image whose properties allows us to characterize them as either inclusions or autofluorescence. Figure 1 displays a small animal with fluorescent probes targeting cancer, and Figure 2 a model exhibiting a target and interference generated by simulated autofluorescence. A defining characteristic is that inclusions have a relatively high-contrast, well-defined, almost round shape, while autofluorescent objects are characterized by irregular, lower-contrast shapes. In this workshop, several filtering techniques have been implemented to identify the structures, such as wavelet transform, principal component analysis, and normalized cross-correlation and shape fitting.

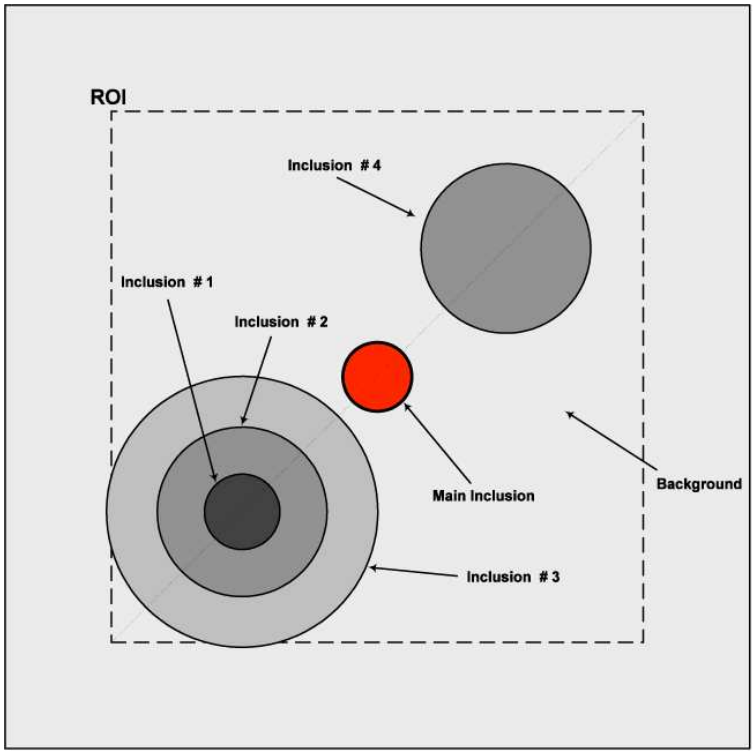

Figure 2. Numerical model exhibiting a target and interference generated by simulated autofluorescence

2. Problem Approaches

2.1. Wavelet Transform

Method

The general denoising procedure using a wavelet transform involves three steps: decompose, threshold, and reconstruct (see [7] and [10]). Firstly, a wavelet transform and a decomposition level N are chosen, and the wavelet decomposition of the signal at the level N is computed. Secondly, for each level from 1 to N, a threshold is selected and soft or hard thresholding is applied to the detail coefficients. Finally, a wavelet reconstruction is computed using the original approximation coefficients of the level N and the modified detail coefficients of levels from 1 to N. When this technique is applied to an image of fluorescence, the reconstructed image can be considered as the main inclusion from targeted probes after extracting the autofluorescence from tissues.

Results

In this project, the wavelet transform approach was carried out by using the Matlab wavelet toolbox [1]. Specifically, we have utilized the 2D discrete stationary wavelet transform (swt2) with "db1" wavelets to carry out the wavelet decomposition. The reconstructed images were produced by the inverse stationary wavelet transform (iswt2) after soft thresholding.

Figure 3 illustrates a 3-level wavelet decomposition on the synthetic image obtained in Case 1 with Detector 1. Figure 4 shows a comparison of one original image and the reconstructed main component of the image using the inverse wavelet transform. Note that the structure of the main inclusion can be identified more easily in the reconstructed image than in the original image.

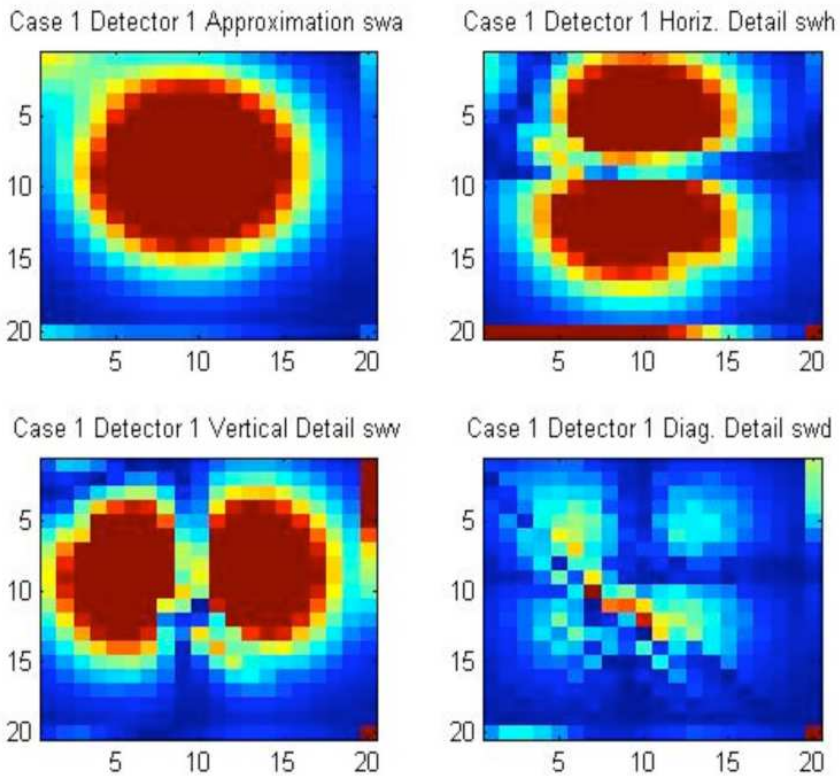

Figure 3. 3-level wavelet decomposition for the synthetic image (case 1 detector 1)

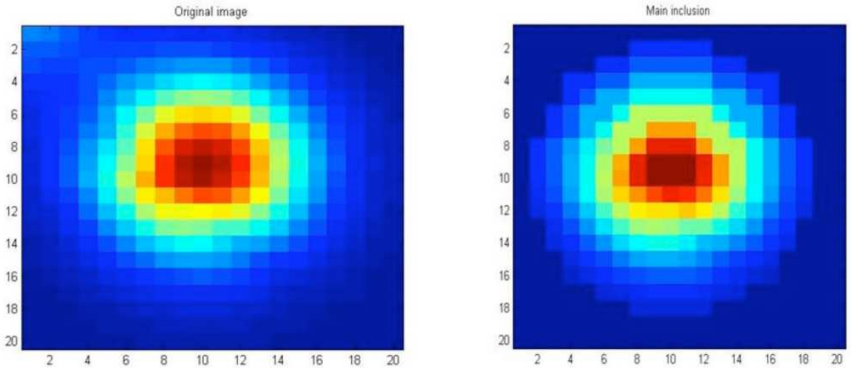

Figure 4. Original and reconstructed image of the main component

Discussion

The well-known wavelet package Wavelab is available at

`http://www-stat.standford.edu/~wavelab/`

(see [2]). Because of the time limitation, we could use the Matlab wavelet toolbox only. It would be interesting to explore the use of Wavelab for extracting autofluorescence from the diffuse optical images. Wavelet thresholding is an efficient technique to filter additive noise and restore original signals. The quality of the reconstructed signal depends on the choice of threshold and the method of thresholding. The specific thresholding strategies should be selected according to the basic

autofluorescence model. Moreover, different thresholding techniques need to be tested in order to determine which method produces the best results for the diffuse optical images of fluorescence.

2.2. Principal Component Analysis

Method

Another way of segmenting the inclusions and other objects in the image is by using a Principal Component Analysis (PCA). Here, it is carried out by performing a Singular Value Decomposition (SVD) and choosing only the components corresponding to the largest singular values (to reveal the most important structures in the image). The image is represented by a matrix A of size $m \times n$. The SVD of A is a matrix factorization of the form $A = USV^t$. Let $s_1 \geq \ldots \geq s_i \geq \ldots \geq s_r \geq 0$ be the singular values of A, where $r = \min(m, n)$. S is diagonal with singular values in non-decreasing order and U and V have orthonormal columns; each column of U (resp. V) is a left-singular (resp. right-singular) vector of A. It is well known that the first p $(1 \leq p \leq r)$ singular values capture the most important features of A. Thus we define the ith component A_i as US_iV^t, where S_i is a matrix obtained from S by zeroing all the diagonal elements except for s_i.

Results

In our experiments, we have empirically chosen the first three components, because they contain almost all the meaningful information. For some images, considering as few as two components is enough. Figure 5 displays the results of the PCA for a synthetic image. In the original image (see Figure 5 top left), one can see an inclusion with some background fluorescence in the upper left corner. Figures 5 top right, 5 bottom left, and 5 bottom right represent the A_1, A_2, and A_3 components, respectively. In this case, the inclusion is almost completely contained in A_1, while the background fluorescence is in A_2. Component A_3 contains some negligible details. For this image, the background fluorescence can be removed easily.

Figure 6 top left demonstrates an image of the mouse with an inclusion (black arrow). You can observe a lot of fluorescence from the organs in addition to the target inclusion. Figures 6 top right, 6 bottom left, and 6 bottom right represent the A_1, A_2, and A_3 components, respectively. In this case, the number of fluorescent objects in the image is relatively large and separating them out is not as straightforward as in the previous example.

Discussion

If any preliminary knowledge about the objects in the image is available, the information from the three components can be combined in a certain way, i.e. $\alpha A_1 + \beta A_2 + \gamma A_3$, where A_1, A_2, and A_3 are the image components, and α, β, and γ the coefficients that reflect the weight of each component. While the success of the PCA segmentation depends on image sophistication, the target inclusion is almost always present in the A_1 component because it has a relatively well-defined shape and shows high-contrast fluorescence. Separating out the components, however, cannot be considered an acceptable solution in many cases, since it often degrades the overall quality of the image. Below we develop a more robust approach, which is capable of separating out objects from the image. Moreover, it does not depend upon the number of the objects and can even handle partially overlapping objects.

2.3. Cross-Correlation and Shape Fitting

Method

In this approach, we try to separate out the elliptical shapes in the image. This is justified by the following assumptions: 1) target inclusions are almost always round, and 2) autofluorescent

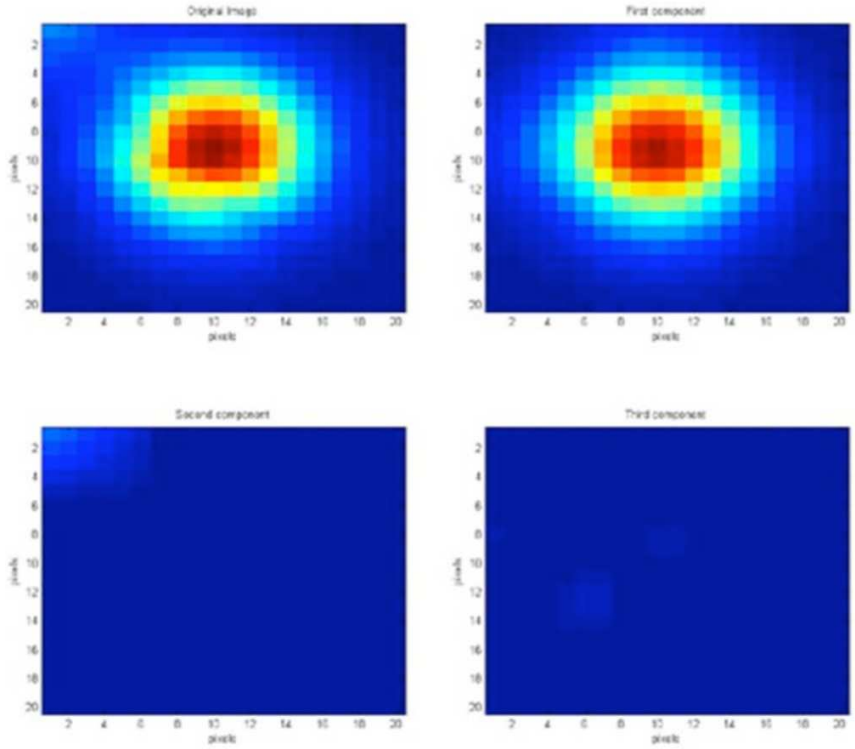

Figure 5. Components of the PCA for the simulated image

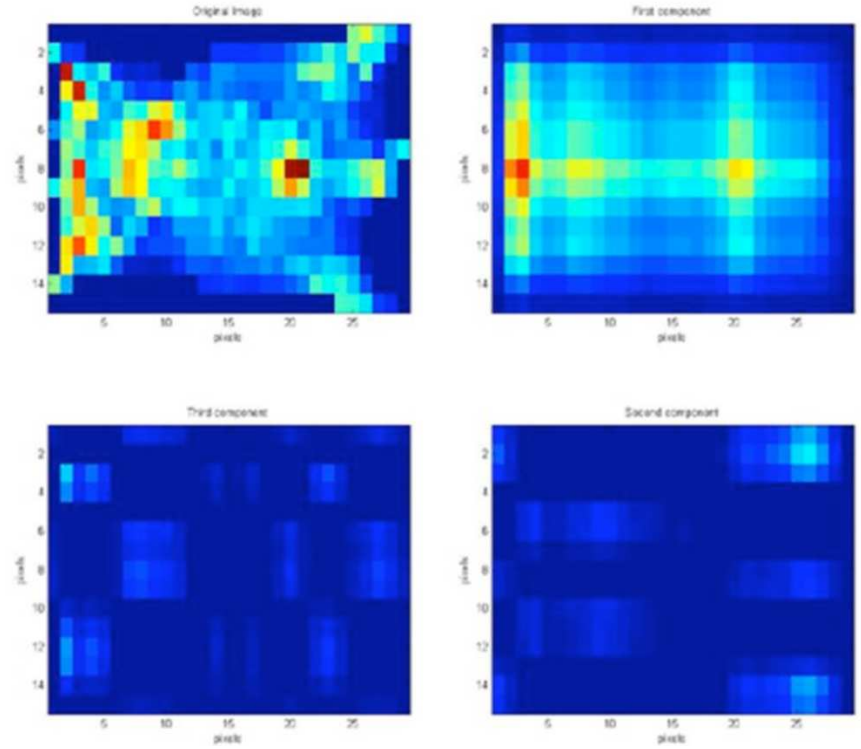

Figure 6. PCA analysis of a real image

objects, though generally of irregular shapes, are low-contrast, and in many cases can be treated as consisting of one or several partially overlapping elliptical shapes. The general idea of the algorithm is to separate out objects from the image one by one, and estimate their shapes to determine what kind of object is extracted at each iteration; the nature of the object will help one decide whether it should be removed from the image or not. As there can be many fluorescent objects, a smaller region of the image is chosen at each iteration. We use a Gaussian model f_p to define an elliptical shape: $f_p(x,y) = v_0 + v_1 e^{-s(x,y)}$, where $s(x,y)$ is defined as $a_1(x-b_x)^2 + 2a_2(x-b_x)(y-b_y) + a_3(y-b_y)^2$, x and y are the coordinates of the pixels in the image, (b_x, b_y) is the centre of the bump, and a_1, a_2, and a_3 define the elliptical shape. Note that $a_1 a_3 - a_2^2 > 0$. We choose several highly probable bump sizes and compute the location of the bumps in the image by maximizing normalized cross-correlation of the model and the image data. Then we choose the parameters of the bump that conform to the largest number of template sizes or to the one containing the brightest pixels. These estimated parameters serve as a first guess for refining the optimization procedure.

In order to remove the bump from the image, we fit the image data $\Phi_{x,y}$ to the model $f_p(x,y)$ by solving an optimization problem with the model parameters b_x, b_y, a_1, a_2, a_3, v_0, and v_1:

$$\min \|f_p(x,y) - \Phi_{x,y}\|^2.$$

A similar idea, for a different model, is explored in [11], where it is described in more detail.

Results

Figure 7 top left demonstrates a light intensity function from a synthetic image that contains one well defined bump and a background fluorescence caused by another (close) bump. Figure 7 top center shows the fitted model and Figure 7 top right the result of the removal of the detected bump. The remaining bump can be separated from the image in the same fashion. Figure 7 bottom shows the results of a similar procedure carried out on an *in vivo* image of a mouse. At the first iteration a target inclusion was detected (see Figure 7, bottom left and center). Figure 7 bottom right displays the bumps that can be detected at the subsequent iterations of the algorithm.

Discussion

Generally speaking, this algorithm requires a fine tuning of the parameters, based on what is known about imaging data; this is so because the success of the optimization procedure depends on the quality of the first guess. For example, it is useful to have a notion of the possible bump sizes in order to obtain a good fit. The choice of the stopping criteria is another important issue. For instance, the number of iterations may be fixed beforehand in the case where the number of extracted objects is known or can be guessed reasonably well. On the other hand, the algorithm may be stopped if it can be inferred from the image or bump parameters that there are no inclusions or autofluorescent objects left in the image.

References

1. *Matlab wavelet toolbox documentation.*
2. `http://www-stat.stanford.edu/~wavelab`.
3. S. Achilefu, R. Dorshow, J. Bugaj, and R. Rajagopalan, *Novel receptor-targeted fluorescent contrast agents for* in-vivo *tumor imaging*, Invest. Radiol. **35** (2000), 479–485.
4. D. A. Boas, G. Strangman, J. P. Culver, R. D. Hoge, G. Jasdzewski, R. A. Poldrack, B. R. Rosen, and J. B. Mandeville, *Can the cerebral metabolic rate of oxygen be estimated with near-infrared spectroscopy?*, Physics in Medicine and Biology **48** (2003), 2405–2418.
5. J. P. Culver, A. M. Siegel, J. J. Stott, and D. A. Boas, *Volumetric diffuse optical tomography of brain activity*, Optics Letters **28** (2003), no. 21, 2061–2063.

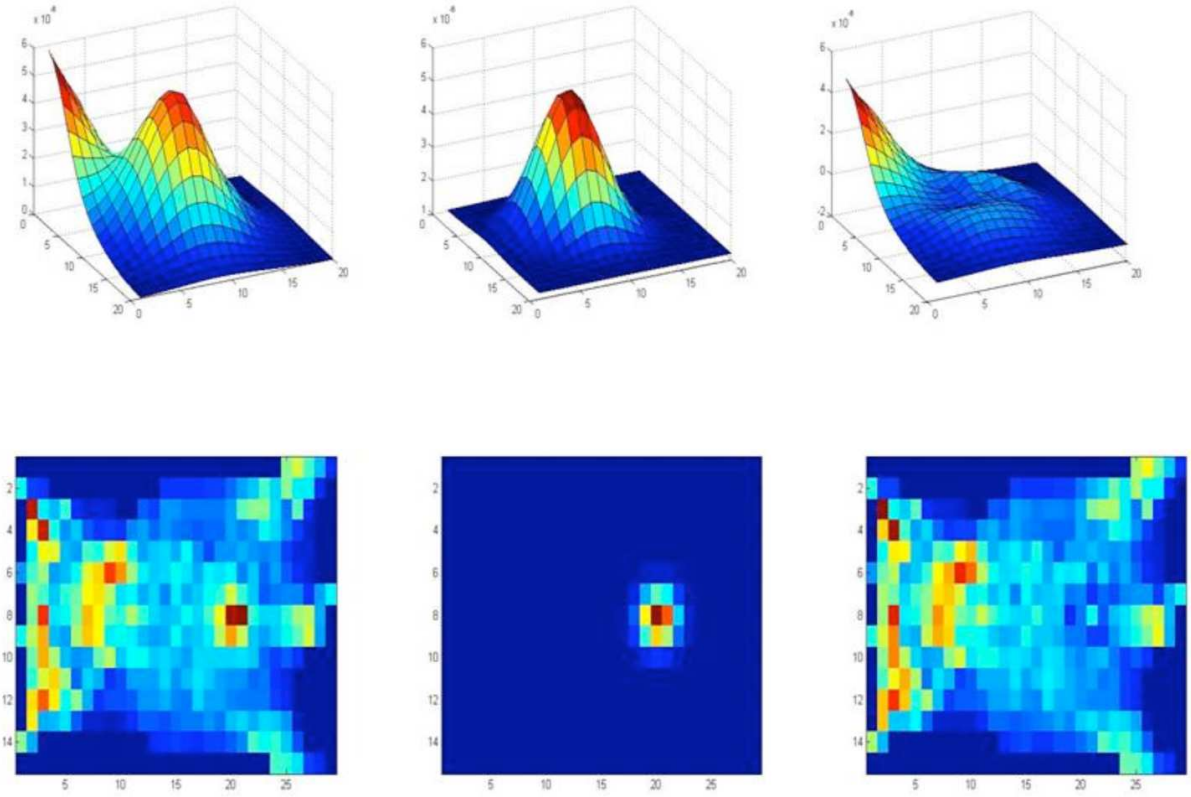

Figure 7. Results of the cross-correlation technique

6. J. V. Frangioni, *In vivo near-infrared fluorescence imaging*, Curr. Opin. Chem. Biol. **7** (2003), 626–634.
7. A. Graps, *An introduction to wavelets*, IEEE **2** (1995), no. 2.
8. X. Intes and B. Chance, *Non-PET functional imaging techniques: optical*, Radiologic Clinics of North America **43** (2005), 221–234.
9. K. Licha, *Contrast agents for optical imaging*, Topics in Current Chemistry **222** (2002), 1–29.
10. Stéphane Mallat, *A wavelet tour of signal processing*, 2nd edition, Academic Press, 1999.
11. O. Peshko, C. Anand, and T. Terlaky, *Surface reconstruction from structured-light images for radiation therapy*, Photonic Applications in Biosensing and Imaging, Proceedings of SPIE, no. 5969, 2005, pp. 427–436.
12. R. Weissleder and U. Mahmood, *Molecular imaging*, Radiology **219** (2001), 316–333.
13. A. Yodh and B. Chance, *Spectroscopy and imaging with diffusing light*, Phys. Today **48** (1995), 34–40.
14. G. Zheng, Y. Chen, X. Intes, B. Chance, and J. Glickson, *Contrast-enhanced NIR optical imaging for subsurface cancer detection*, J. Porphyrin and Phthalocyanines **8** (2004), 1106–1118.